NeuroImage: Clinical 19 (2018) 572–580

Contents lists available at ScienceDirect

NeuroImage: Clinical

journal homepage: www.elsevier.com/locate/ynicl

Diffusion MRI tractography for improved transcranial MRI-guided focused ultrasound thalamotomy targeting for essential tremor

Qiyuan Tian[a,b,*], Max Wintermark[b], W. Jeffrey Elias[c], Pejman Ghanouni[b], Casey H. Halpern[d], Jaimie M. Henderson[d], Diane S. Huss[e], Maged Goubran[b], Christian Thaler[b,f], Raag Airan[b], Michael Zeineh[b], Kim Butts Pauly[a,b], Jennifer A. McNab[b]

[a] Department of Electrical Engineering, Stanford University, Stanford, CA, United States
[b] Department of Radiology, Stanford University, Stanford, CA, United States
[c] Department of Neurosurgery, University of Virginia, Charlottesville, VA, United States
[d] Department of Neurosurgery, Stanford University, Stanford, CA, United States
[e] Department of Physical Therapy, University of Virginia, Charlottesville, VA, United States
[f] Department of Diagnostic and Interventional Neuroradiology, University Medical Center Hamburg-Eppendorf, Hamburg, Germany

ARTICLE INFO

Keywords:
Transcranial MRI-guided focused ultrasound
Thalamotomy
Essential tremor
Diffusion tractography
Neurosurgical targeting
Ventral intermediate nucleus

ABSTRACT

Purpose: To evaluate the use of diffusion magnetic resonance imaging (MRI) tractography for neurosurgical guidance of transcranial MRI-guided focused ultrasound (tcMRgFUS) thalamotomy for essential tremor (ET).
Materials and methods: Eight patients with medication-refractory ET were treated with tcMRgFUS targeting the ventral intermediate nucleus (Vim) of the thalamus contralateral to their dominant hand. Diffusion and structural MRI data and clinical evaluations were acquired pre-treatment and post-treatment. To identify the optimal target location, tractography was performed on pre-treatment diffusion MRI data between the treated thalamus and the hand-knob region of the ipsilateral motor cortex, the entire ipsilateral motor cortex and the contralateral dentate nucleus. The tractography-identified locations were compared to the lesion location delineated on 1 year post-treatment T_2-weighted MR image. Their overlap was correlated with the clinical outcomes measured by the percentage change of the Clinical Rating Scale for Tremor scores acquired pre-treatment, as well as 1 month, 3 months, 6 months and 1 year post-treatment.
Results: The probabilistic tractography was consistent from subject-to-subject and followed the expected anatomy of the thalamocortical radiation and the dentatothalamic tract. Higher overlap between the tractography-identified location and the tcMRgFUS treatment-induced lesion highly correlated with better treatment outcome ($r = -0.929, -0.75, -0.643$, $p = 0.00675, 0.0663, 0.139$ for the tractography between the treated thalamus and the hand-knob region of the ipsilateral motor cortex, the entire ipsilateral motor cortex and the contralateral dentate nucleus, respectively, at 1 year post-treatment). The correlation for the tractography between the treated thalamus and the hand-knob region of the ipsilateral motor cortex is the highest for all time points ($r = -0.719, -0.976, -0.707, -0.929$, $p = 0.0519, 0.000397, 0.0595, 0.00675$ at 1 month, 3 months, 6 months and 1 year post-treatment, respectively).
Conclusion: Our data support the use of diffusion tractography as a complementary approach to current targeting methods for tcMRgFUS thalamotomy.

1. Introduction

Essential tremor (ET) is one of the most common neurological diseases, currently affecting an estimated seven million individuals in the United States and millions more worldwide (Louis et al., 1998; Louis and Ferreira, 2010; Louis and Ottman, 2014). ET patients suffer from physical symptoms, such as rhythmic trembling of the hands, head, voice, legs or trunk, that compromise daily living ability, as well as psychosocial effects that compromise quality of life (Lorenz et al., 2006; Woods et al., 2008; Lorenz et al., 2011). Tremor suppression can be achieved by lesioning or stimulating a relay nucleus of the thalamus, known as the ventral intermediate nucleus (Vim) (Zesiewicz et al., 2005; Fang et al., 2016). One approach to lesion Vim is transcranial magnetic resonance imaging (MRI)-guided focused ultrasound

* Corresponding author at: Departments of Electrical Engineering and Radiology, Stanford University, Richard M. Lucas Center for Imaging, 1201 Welch Road, Stanford, CA 94305, United States.
E-mail address: qytian@stanford.edu (Q. Tian).

https://doi.org/10.1016/j.nicl.2018.05.010
Received 21 September 2017; Received in revised form 3 May 2018; Accepted 8 May 2018
Available online 09 May 2018

(tcMRgFUS). This technique applies a high-intensity focused ultrasound beam to thermally ablate targeted tissue using MRI for guidance (Ghanouni et al., 2015). A key benefit of the tcMRgFUS approach is that it is minimally invasive without the need to open the skull. Thus far, tcMRgFUS has successfully treated ET patients in several clinical trials (Elias et al., 2013; Wintermark et al., 2014a; Wintermark et al., 2014b; Elias et al., 2016; Schreglmann et al., 2017).

Accurate targeting of Vim is essential for safe, effective and durable treatment with tcMRgFUS. Vim is a relatively small structure (approximately $4 \times 4 \times 6\,mm^3$ (Nowinski et al., 2008; Sammartino et al., 2016)) and has low intrinsic contrast relative to surrounding thalamic nuclei on standard structural MRI (Tourdias et al., 2014; Saranathan et al., 2015). Current methods to target Vim use a standard atlas overlaid on the patients' structural MR images or stereotactic location derived from population-based coordinates relative to the anterior commissure-posterior commissure line (Ghanouni et al., 2015). These methods have several limitations. First, they do not account for all of the anatomical variability between subjects (Kincses et al., 2012). Second, they lack specificity. For example, identification of the hand representation within Vim, is of particular interest to more specifically treat hand tremor symptoms. Improvements in patient-specific, image-based targeting for tcMRgFUS could also help to minimize adjustments of the target based on real-time patient feedback during the procedure, which can result in prolonged treatment time and a risk of adverse effects such as edema spreading into the nearby capsule.

By mapping the white matter pathways that conduct the electrical signals governing hand movement, we hypothesize that diffusion MRI tractography (Conturo et al., 1999; Mori et al., 1999; Behrens et al., 2007; Morris et al., 2008; Descoteaux et al., 2009; Ye et al., 2016; Pujol et al., 2015) can help identify a location in the thalamus that maximizes the reduction of hand shaking, minimizes side effects, and shortens the procedure time. Diffusion MRI tractography is a non-invasive technique that reconstructs three-dimensional models of white matter fiber pathways based on voxel-wise diffusion patterns (Basser et al., 1994; Pierpaoli and Basser, 1996; Tuch et al., 2002; Behrens et al., 2003a; Tournier et al., 2004; Wedeen et al., 2005; Jbabdi et al., 2012) measured by a diffusion-sensitized MRI acquisition (Stejskal and Tanner, 1965). Diffusion tractography algorithms can be divided into deterministic (Conturo et al., 1999; Mori et al., 1999) and probabilistic (Behrens et al., 2007; Morris et al., 2008; Descoteaux et al., 2009) approaches. Models of the voxel-wise diffusion pattern can be generally divided into those that take into account intra-voxel crossing fibers (Tuch et al., 2002; Behrens et al., 2003a; Tournier et al., 2004; Wedeen et al., 2005; Jbabdi et al., 2012; Tian et al., 2016) and those that do not, such as the traditional single fiber diffusion tensor model (Basser et al., 1994; Pierpaoli and Basser, 1996).

Tractography has been applied previously to segment the nuclei of the thalamus by mapping the structural connections between the thalamus and distinct cortical areas (Behrens et al., 2003b; Pouratian et al., 2011; Elias et al., 2012). This methodology was validated using architectonic atlases, functional MRI (Johansen-Berg et al., 2005) and electroencephalography (Elias et al., 2012) and was shown to have high within-subject and between-subject reproducibility (Behrens et al., 2003b; Traynor et al., 2010). A subset of cortical areas is commonly used to reconstruct white matter tracts that intersect with specific thalamic regions of interest based on known thalamocortical structural connections. For example, tracer studies have shown that Vim is the primary location within the thalamus that connects with motor cortex (Rouiller et al., 1999; Rouiller et al., 1994; Sakai et al., 2002; Stepniewska et al., 2003; Schell and Strick, 1984; Wiesendanger and Wiesendanger, 1985; Jones et al., 1979; Matelli et al., 1989; Darian-Smith et al., 1990). Tractography studies have replicated this anatomy by tracking between the thalamus and the primary motor cortex (Kincses et al., 2012; Jakab et al., 2016) or between the red nucleus and motor cortex (Yamada et al., 2010) to target Vim. Prior studies have evaluated the efficacy of tractography-based Vim targeting on healthy subjects by comparison to an atlas or inter-subject reproducibility (Kincses et al., 2012; Jakab et al., 2016; Yamada et al., 2010). The predominant application of tractography-based targeting is deep brain stimulation (DBS) surgery (Sammartino et al., 2016; Kincses et al., 2012; Pouratian et al., 2011; Elias et al., 2012; Barkhoudarian et al., 2010; Sedrak et al., 2011; Klein et al., 2012; Akram et al., 2018) (review papers: (Henderson, 2012; Torres et al., 2014; Calabrese, 2016)).

Here, we evaluate diffusion tractography as a neurosurgical guidance tool specifically in the context of tcMRgFUS treatment. Our retrospective study involves eight ET patients treated in a clinical trial at Stanford University. We retrospectively identified a target location using pre-treatment diffusion tractography data and compared the tractography-identified location with the location where the lesion had been induced. The overlap between the tractography-identified location and the lesion was correlated with the clinical outcomes to evaluate the utility of the tractography targeting procedure for future prospective studies. We mapped three different tracts by performing the probabilistic tractography for identifying the Vim, i.e. between the treated thalamus and the hand-knob region (Yousry et al., 1997) of the ipsilateral motor cortex, the entire ipsilateral motor cortex and the contralateral dentate nucleus. Our study is also distinguished from prior literature by correlating with clinical outcomes measured at time points that extend to one full year from the time of treatment and accounting for the uncertainty of the probabilistic tractography results to identify the targeted region.

2. Materials and methods

2.1. Study population and procedure

The study was conducted with institutional review board approval of Stanford University. Prospective, informed consent was provided by the patients enrolled in the study. Eight patients with bilateral medication-refractory ET were treated with tcMRgFUS thalamotomy targeting Vim contralateral to their dominant hand at Stanford University (details of the inclusion and exclusion criteria described in (Federau et al., 2017)). Lesioning was performed using a clinical 3 Tesla MRI system (Discovery MR750, GE Healthcare, Milwaukee, Wisconsin) and a clinical system for focused ultrasound surgery (ExAblate Neuro 4000, InSightec, Haifa, Israel). Diffusion MRI data were not used for targeting in these treatments, rather traditional indirect targeting was performed. Specifically, the Vim location was initialized by referring to the anterior commissure-posterior commissure line, and further adjusted and confirmed using intra-procedural feedback from awake patients such that the hand tremor was maximally suppressed and unwanted side effects minimized (Ghanouni et al., 2015; Elias et al., 2016).

2.2. Clinical outcome assessment

All patients were clinically evaluated by the same neurologist based on recorded patient videos and drawings/hand writings from pre-treatment, as well as 1 month, 3 months, 6 months and 1 year post-treatment. The 1 year score for patient P3 was not available. The efficacy of tremor suppression was measured using the Clinical Rating Scale for Tremor (CRST) (Fahn et al., 1993), which consists of three components: Part A (tremor severity), Part B (specific motor task performance) and Part C (functional disability resulting from tremor). A hand-specific sub-score of a combined A + B score for the treated hand (ranging from 0 to 32) was used to compare to the tractography results. Higher scores indicate worse tremor.

2.3. MRI protocol

MRI scans were performed on a clinical 3 Tesla MRI system (Discovery MR750, GE Healthcare, Milwaukee, Wisconsin) equipped with an 8-channel radio frequency receive coil. Data acquisition

Table 1
MRI data acquisition sequences and parameters. DW-SE-EPI = diffusion-weighted spin-echo echo-planar imaging; FSE = fast spin echo; MPRAGE = magnetization-prepared rapid gradient-echo; TE = echo time; TR = repetition time; TI = inversion time; TS = shot interval time; ASSET = array coil spatial sensitivity encoding; ARC = autocalibrating reconstruction for Cartesian imaging.

	Diffusion-weighted	T_2-weighted	T_1-weighted
Sequence	2D single-refocused DW-SE-EPI	3D FSE	MPRAGE
TE/TR (ms)	81.6/8500	83.5/2500	3.73/8.3/1100 (TI)/3000 (TS)
Flip angle (°)	90	90	9
Field-of-view (mm^2)	240 × 240	240 × 240	180 × 180
Matrix size	128 × 128	320 × 320	180 × 180
In-plane res. (mm^2)	1.875 × 1.875	0.75 × 0.75	1 × 1
Slice thickness (mm)	2	1	1
Slice spacing (mm)	0	0.5	0.5
Number of slice	69 axial	180 sagittal	220 coronal
Parallel imaging	ASSET factor = 2	ARC factor = 2	ARC factor = 2
Acq. time (min)	10	7	3.5
Diffusion encoding	6 × b = 0 60 directions × b = 2500 s/mm^2		

included whole-brain diffusion and structural MRI data. Diffusion-weighted MRI data were acquired pre-treatment using a two-dimensional (2D) single-refocused diffusion-weighted spin-echo echo-planar imaging (DW-SE-EPI) sequence. T_2-weighted and T_1-weighted MRI data were acquired 1 year post-treatment using a three-dimensional (3D) fast spin echo (FSE) sequence and a 3D magnetization-prepared rapid gradient-echo (MPRAGE) respectively. Data acquisition parameters are shown in Table 1.

2.4. Regions of interest

Regions-of-interest (ROIs) for diffusion tractography were obtained from the automated volumetric segmentation of the FreeSurfer software (Dale et al., 1999; Fischl et al., 1999) (https://surfer.nmr.mgh.harvard.edu/) and manual delineation. Cortical surface reconstruction and volumetric segmentation was performed on the 1 year post-treatment T_1-weighted data using FreeSurfer. Binary masks of the sub-cortical white matter of the precentral gyrus (Fig. 1a) and the corpus callosum were extracted from FreeSurfer's white matter parcellation (i.e. wmparc.mgz).

Binary masks of the thalamus (Fig. 1a) and sub-cortical white matter of the hand-knob region of the motor cortex (Fig. 1a) were manually drawn by a neuroradiologist (M.W.). Binary masks of the dentate nucleus, red nucleus and the superior cerebellar peduncle (Fig. 1a) were manually drawn by a neuroradiologist (C.T.). The manual delineation was based on the non-diffusion weighted (b = 0) image and the fractional anisotropy map from the pre-treatment diffusion MR data.

The tcMRgFUS treatment-induced lesion was delineated by a neuroradiologist (M.W.) on the T_2-weighted images 1 year post-treatment to encompass the Zones 1 and 2 (Wintermark et al., 2014a) (Fig. 1b).

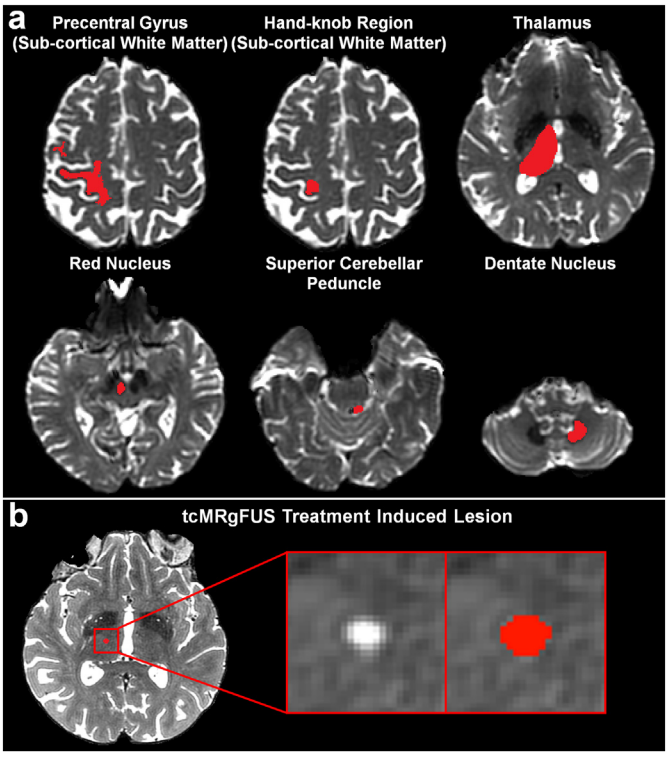

Fig. 1. Example of binary masks (red) of regions-of-interests (ROIs) used to perform diffusion tractography (a) and tcMRgFUS treatment induced lesion (b) from a representative patient (P2). The tractography ROIs were overlaid on the axial slice of b = 0 image from the pre-treatment diffusion data. The lesion ROI was overlaid on the axial slice of post-treatment T_2-weighted image. (For interpretation of the references to color in this figure legend, the reader is referred to the web version of this article.)

2.5. Diffusion tractography

Pre-treatment diffusion images were corrected for eddy current distortions and bulk motion and co-registered using the "eddy" function (cubic eddy current model, 24 iterations, other parameters as default) from the FMRIB Software Library (Jenkinson et al., 2012) (FSL, http://fsl.fmrib.ox.ac.uk/fsl/fslwiki/). The diffusion tensor model was fitted on pre-processed diffusion data using FSL's "dtifit" function to derive the fractional anisotropy map for delineating ROIs. The "ball and stick" model was fitted using FSL's "bedpostx" function (three sticks, other parameters as default) to estimate voxel-wise crossing fiber orientation distributions for probabilistic tractography.

Probabilistic tractography was performed using FSL's "probtrackx2" functions in three different ways:

(1) thalamus to hand-knob: the treated thalamus as the "seed", the ipsilateral hand-knob region of the motor cortex as the "target";
(2) thalamus to motor: the treated thalamus as the "seed", the sub-cortical white matter of the ipsilateral precentral gyrus as the "target";
(3) thalamus to dentate: the treated thalamus as the "seed", the contralateral dentate nucleus as the "target", the ipsilateral red nucleus and the contralateral superior cerebellar peduncle as waypoints.

The corpus callosum was used as the exclusion mask for all three

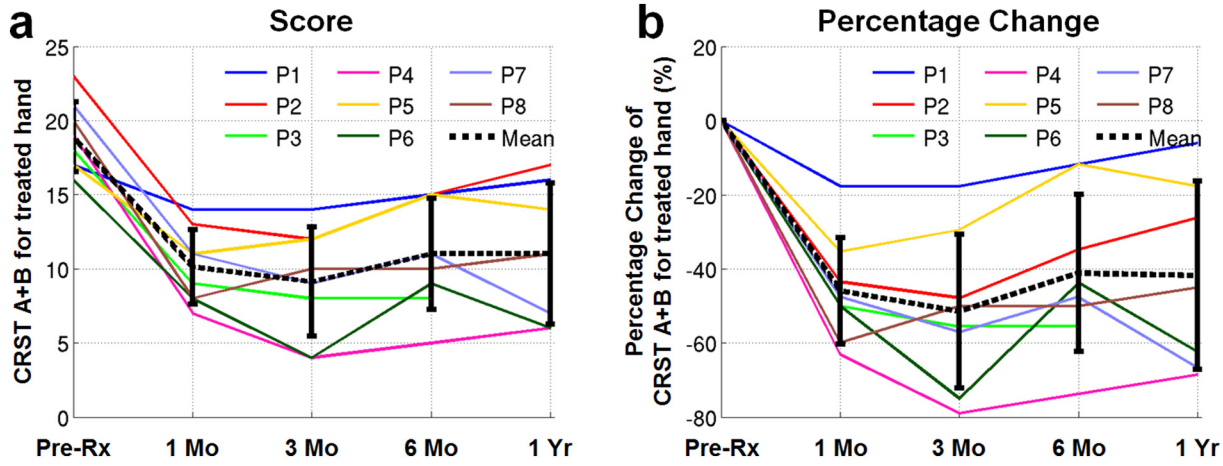

Fig. 2. Clinical outcomes of hand tremor suppression measured by the Clinical Rating Scale for Tremor (CRST) A + B sub-score for the treated hand at 1 month, 3 months, 6 months and 1 year (a) and the percentage change compared to the pre-treatment score (b). The colored lines display scores for individual patients. The black dashed lines and the black solid error bar display the group mean scores and the standard deviations (mean ± standard deviation) of the scores, respectively, at each time point. (For interpretation of the references to color in this figure legend, the reader is referred to the web version of this article.)

methods. For patient P1, tractography was further performed for the untreated thalamus.

The classification option of "probtrackx2" was used to determine the number of streamlines from each thalamic voxel that reach the targeting region (5000 streamlines were initialized from each thalamic voxel). The streamline count is a measure of the probability that a reconstructed pathway can be found between a given thalamic voxel and the targeting region. For each patient, the streamline count in each thalamic voxel was normalized by the total number of streamlines between the entire thalamus and the targeting region (called "waytotal" number) for group analysis.

For volume rendering of tractography results (Figs. 3, 5), a threshold of 1% was used to binarize the probabilistic tractography. For visualization of the normalized streamline count (Figs. 4, 5), a window of [0, 0.3%], [0, 0.2%] and [0, 1%] was used for the thalamus to hand-knob, thalamus to motor and thalamus to dentate tracts respectively. The windows and thresholds were used for visualization purpose only. No windows or thresholds were used for any of the statistical analyses.

2.6. Image co-registration

Image co-registration was performed using the NiftyReg software (https://cmiclab.cs.ucl.ac.uk/mmodat/niftyreg) (Modat et al., 2010; Modat et al., 2014). The pre-treatment diffusion image was co-registered to the post-treatment T_2-weighted image in a two-step fashion. Specifically, the pre-treatment diffusion image (b = 0) was first linearly registered to the post-treatment T_2-weighted image using NiftyReg's "reg_aladin" function (default parameters). The transformed diffusion image was then non-linearly registered to the post-treatment T_2-weighted image using NiftyReg's "reg_f3d" function (default parameters). The affine and non-linear transformations were inversed and integrated into a single transformation using NiftyReg's "reg_transform" function to transform the binary mask of the lesion ROI delineated on the post-treatment T_2-weighted image to the pre-treatment diffusion image using nearest-neighbor interpolation. The non-linear co-registration method was utilized to account for the susceptibility artifact induced distortion present in the diffusion images.

The pre-treatment diffusion image was co-registered to the post-treatment T_1-weighted images by concatenating the transformation between the pre-treatment diffusion image and the post-treatment T_2-weighted image, and the transformation between the post-treatment T_2-weighted image and the post-treatment T_1-weighted image (obtained in the aforementioned two-step fashion using NiftyReg) using NiftyReg's "reg_transform" function. The concatenated transformation was used to transform the binary masks of FreeSurfer's automated segmentation results (i.e. sub-cortical white matter of pre-central gyrus and the corpus callosum) to the pre-treatment diffusion image using nearest-neighbor interpolation.

The registration results were visually confirmed for quality control. In addition, the cross-correlation between the pre-treatment diffusion image (b = 0) and the co-registered T_2-weighted (0.9872 ± 0.0012) and T_1-weighted images (0.9406 ± 0.0093) computed using the "MeasureImageSimilarity" function from the Advanced Normalization Tools (ANTs, http://stnava.github.io/ANTs) (Avants et al., 2011) was used to quantify the image similarity and ensure the quality of image co-registration.

2.7. Statistical analysis

Non-parametric Wilcoxon signed-rank test was performed for two related samples to evaluate differences between values at baseline and at each of the four assessments after treatment, as well as differences in scores over time. The total probabilistic streamline count within the lesion was used as a measure of overlap between the tractography-identified location and the tcMRgFUS treatment-induced lesion. The streamline count was correlated with the percentage change of CRST A + B hand sub-score at 1 month, 3 months, 6 months and 1 year post-treatment compared to pre-treatment score. The Pearson product-moment correlation coefficient, p-value, and 95% bootstrap confidence interval of the correlation coefficient (5000 bootstrap samples) were calculated to quantify the linear correlation. Statistical analysis was performed using MATLAB software (MathWorks, Natick, Massachusetts).

3. Results

3.1. Clinical outcome

The tremor in the treated hand was suppressed after the treatment as measured by the CRST A + B score (Fig. 2). The CRST A + B score of all patients decreased significantly immediately following the treatment, from 18.88 ± 2.36 pre-treatment to 10.13 ± 2.53 one month post-treatment (−45.90% ± 14.40% reduction, p = 0.0078). From 1 month to 3 months, the CRST A + B score further decreased for P2, P3, P4, P6 and P7, while plateaued or slightly increased for P1, P5 and P8. For all patients, the CRST A + B score increased from 3 months to 6 months (from 9.13 ± 0.92 to 11.00 ± 3.74, 28.67% ± 40.48% increase, p = 0.0312). At 1 year post-treatment, the CRST A + B score of

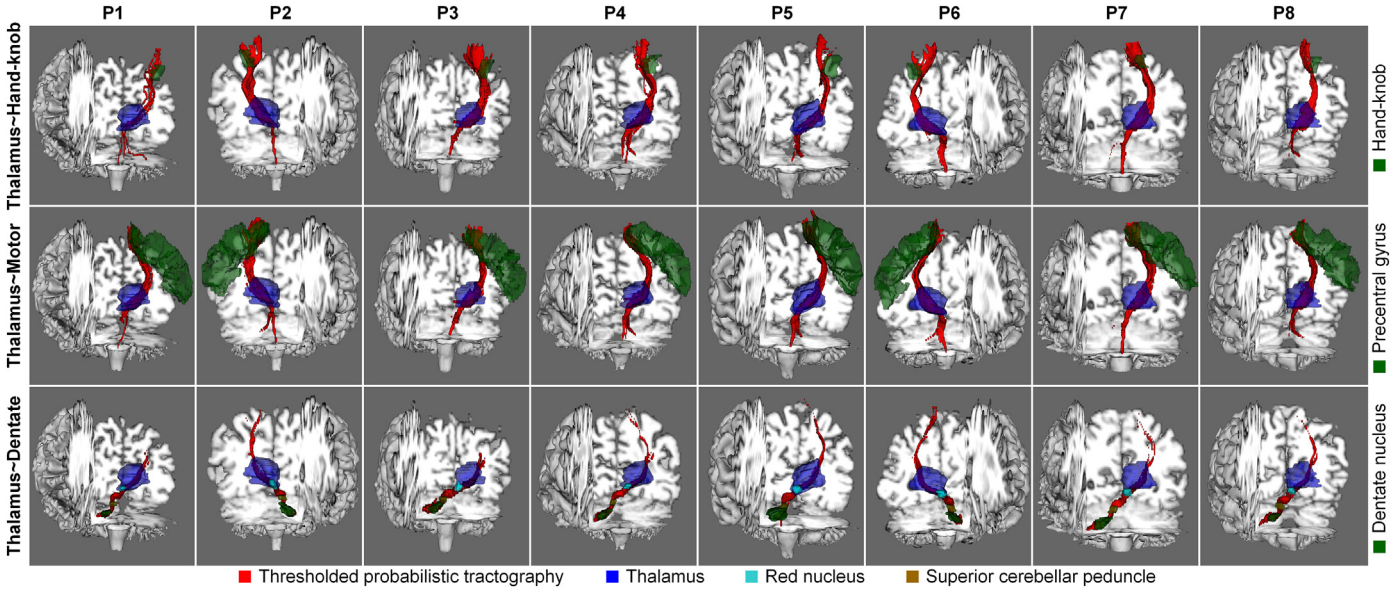

Fig. 3. Thresholded (1% threshold) and volume rendered probabilistic tractography results (red) with the treated thalamus (blue) and targeting regions (green). (For interpretation of the references to color in this figure legend, the reader is referred to the web version of this article.)

all patients decreased from pre-treatment, from 18.88 ± 2.36 pre-treatment to 11.00 ± 4.76 one year post-treatment (−41.74% ± 25.45% reduction, p = 0.0078).

3.2. Diffusion MR tractography

Fig. 3 displays the thresholded and volume rendered tractography results (red volume) between the treated thalamus (blue volume) and the three targeting regions (green volume). The tractography is visually consistent from patient-to-patient and follows the expected anatomy of the thalamocortical radiation (Fig. 3 first and second rows) and the dentatothalamic tract (Fig. 3 third row). Patient P1 exhibits only a few streamlines between the thalamus and the hand-knob region (8 streamlines compared to 20,379–1,385,041 streamlines for P2–P8).

Fig. 4 displays the normalized probabilistic streamline count map (red-yellow area) within the treated thalamus (blue area) overlaid on axial slices from pre-treatment diffusion (b = 0) images through the center of the lesion. The location of thalamic voxels with high probabilistic streamline counts (yellow locations) is visually similar from patient-to-patient. For patients P1, the extremely low number of streamlines reconstructed between the thalamus and the hand-knob region causes the locations with high probabilistic streamline counts in the thalamus to be sparse.

The high-probability area identified by the tractography between the thalamus and the hand-knob region (Fig. 4 first row) is a sub-portion of the high-probability area identified by the tractography between the thalamus and the entire motor cortex (Fig. 4 second row). The locations identified by the thalamocortical radiation (Fig. 4 first and second rows) and the dentatothalamic tract (Fig. 4 third row) are different but overlap.

The green contours in Fig. 4 outline the lesion locations delineated and transformed from the post-treatment structural images. There is considerable overlap between the tractography-identified locations and the tcMRgFUS treatment-induced lesions with the exceptions such as patient P5.

Fig. 5 displays additional tractography results for the untreated thalamus of patient P1. The tractography follows the expected anatomy of the thalamocortical radiation (Fig. 5 first and second columns) and the dentatothalamic tract (Fig. 5 third column). The number of streamlines between the thalamus and the hand-knob region in the untreated hemisphere is significant higher than in the treated hemisphere (8019 vs. 8 streamlines for P1).

3.3. Correlation between tractography and CRST scores

Fig. 6 shows scatter plots (with correlation coefficient, p-value, confidence interval of the correlation coefficient) for the probabilistic streamline count within the tcMRgFUS treatment-induced lesion versus the percentage change of CRST A + B score for the treated hand at 1 month (Fig. 6a, e, i), 3 months (Fig. 6b, f, j), 6 months (Fig. 6c, g, k) and 1 year (Fig. 6d, g, l) post-treatment. These plots demonstrate strong correlation between patients with higher probabilistic streamline counts within the tcMRgFUS treatment-induced lesion (i.e. larger overlap) and better treatment outcomes (i.e. larger percentage change of CRST score). The correlation coefficients are r = −0.929, −0.75, −0.643, p = 0.00675, 0.0663, 0.139 for the tractography between the treated thalamus and the hand-knob region of the ipsilateral motor cortex, the entire ipsilateral motor cortex and the contralateral dentate nucleus, respectively, at 1 year post-treatment. The correlation for the tractography between the treated thalamus and the hand-knob region of the ipsilateral motor cortex is the highest for all time points (r = −0.719, −0.976, −0.707, −0.929, p = 0.0519, 0.000397, 0.0595, 0.00675 at 1 month, 3 months, 6 months and 1 year post-treatment, respectively).

4. Discussion

This study retrospectively evaluates the utility of diffusion tractography for neurosurgical targeting of tcMRgFUS thalamotomy for ET. We build on prior literature that primarily focused on diffusion tractography-based targeting for DBS and extend this line of research to tcMRgFUS. For eight patients, we identified Vim within the treated thalamus by mapping its structural connection to the hand representation of the ipsilateral primary motor cortex, the entire ipsilateral primary motor cortex and the contralateral dentate nucleus using diffusion tractography from pre-treatment data. The overlap between the tractography-identified location and the tcMRgFUS treatment-induced lesion was correlated with clinical outcomes. A strong correlation was found for improved treatment outcomes with increased overlap of the induced lesion and tractography-identified location.

Diffusion MRI tractography offers complementary but intrinsically different information than can be obtained with other types of MRI. It

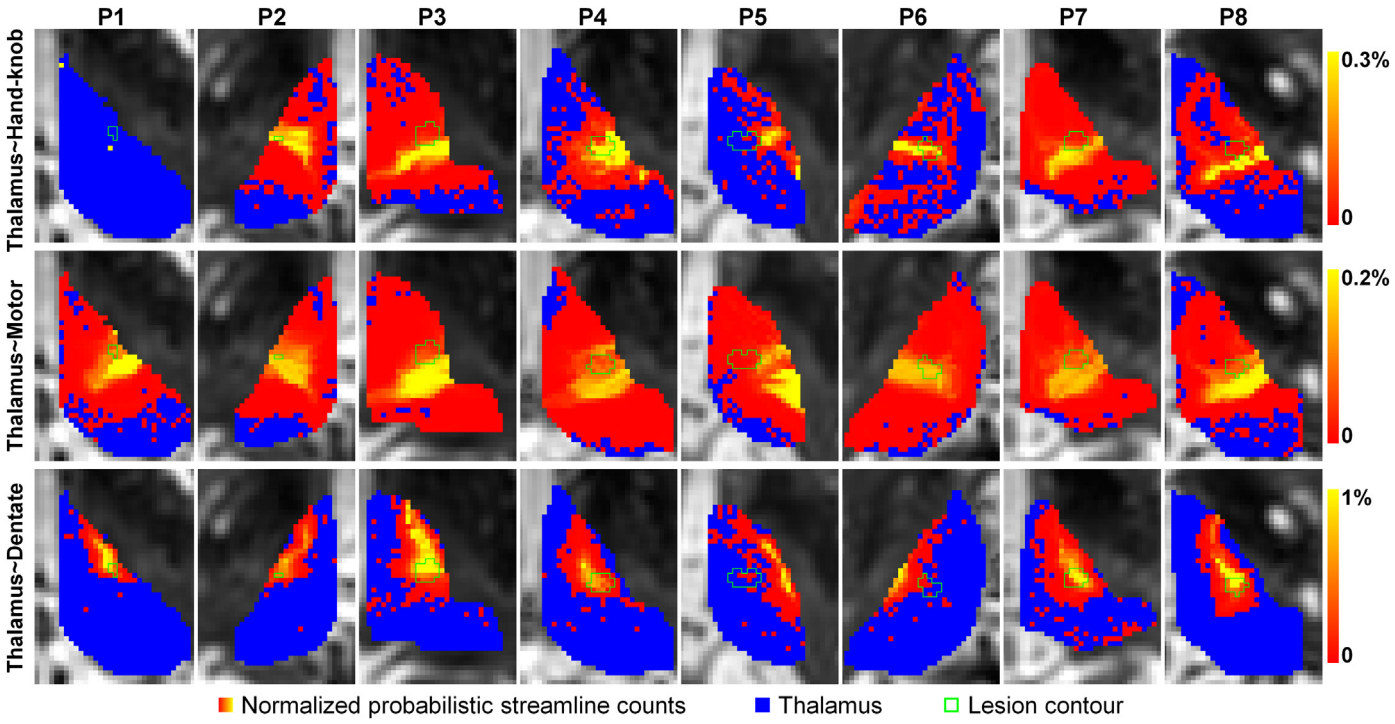

Fig. 4. Maps of normalized probabilistic streamline count (red-yellow) for voxels within the thalamus (blue) overlaid on axial slices from a pre-treatment diffusion b0 image. The green contours display the outline of the tcMRgFUS treatment-induced lesion transformed from post-treatment structural MR images. (For interpretation of the references to color in this figure legend, the reader is referred to the web version of this article.)

maps the white matter pathways important for tremor control within thalamus. Using the hand-knob region of the motor cortex as the target, the tractography is hypothesized to even provide the hand representation within the Vim, which cannot be identified from standard structural MR images, for improved specificity. The location identified by the tract between the thalamus and the hand-knob region of the motor cortex does predict the clinical outcome better than the location identified by the tract between the thalamus and the entire motor cortex (compare Fig. 6 first and second rows). The hand representation within the Vim is of significant interest as the goal of treatment is relief of hand tremor.

Tractography-based targeting results depend on the quality of diffusion MRI data (resolution, b-value, number of diffusion directions, signal-to-noise ratio etc.) and choice of tractography method (Sotiropoulos et al., 2013). Our data acquisition was representative of optimal clinical protocols (2 mm isotropic resolution, 2500 s/mm^2 b-value, 60 directions) for tractography study given a practical scan time of 10 minutes. Similar to most prior studies on tractography-based thalamic segmentation (Pouratian et al., 2011; Elias et al., 2012; Jakab et al., 2016; Klein et al., 2012; Johansen-Berg et al., 2008; Hyam et al.,

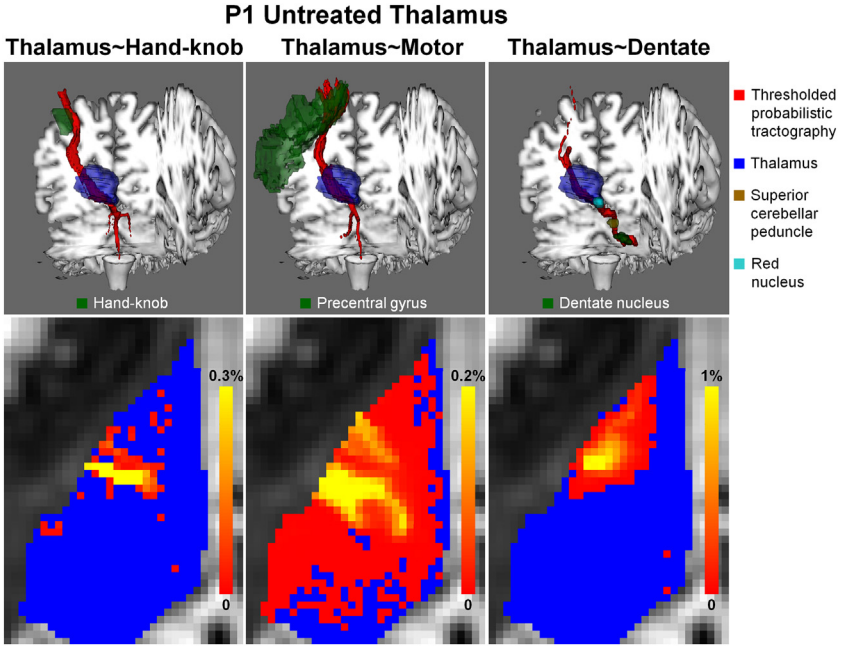

Fig. 5. Tractography results for the untreated thalamus of P1. First row displays the thresholded (1% threshold) and volume rendered probabilistic tractography results (red) with the treated thalamus (blue) and targeting regions (green). Second row displays the map of normalized probabilistic streamline count (red-yellow) of voxels within the thalamus (blue) overlaid on axial slices from pre-treatment diffusion b0 image. (For interpretation of the references to color in this figure legend, the reader is referred to the web version of this article.)

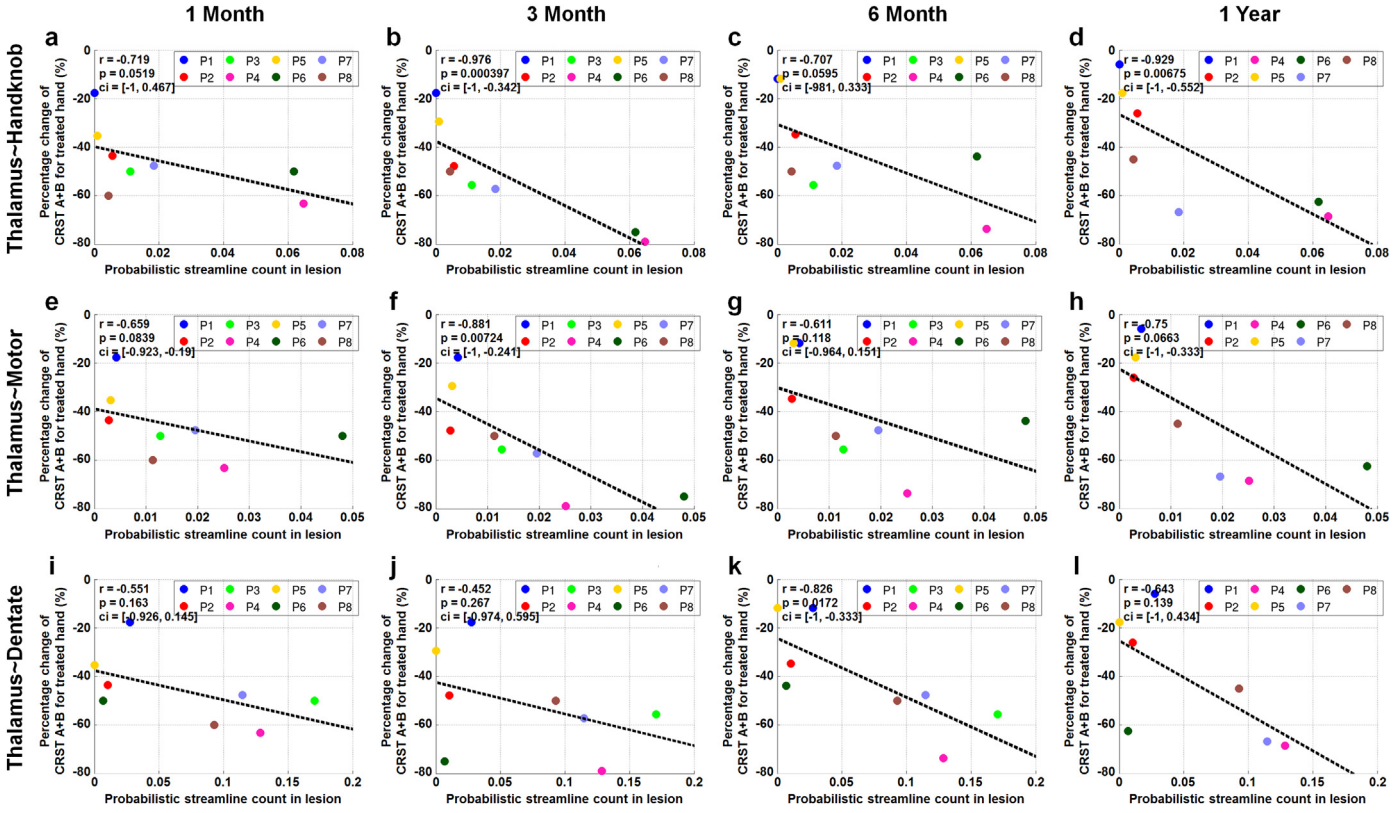

Fig. 6. Scatter plots and fitted lines (with Pearson's correlation coefficient r, p-value p and 95% bootstrap confidence interval ci of r) for the probabilistic streamline count within the tcMRgFUS treatment-induced lesion versus the percentage change relative to pre-treatment of CRST A + B score for the treated hand at 1 month (a, e, i), 3 months (b, f, j), 6 months (c, g, k) and 1 year (d, h, l) post-treatment.

2012), we also used probabilistic tractography and a crossing fiber model in our retrospective study. Probabilistic tractography has the benefit of taking into account noise and uncertainty in the raw data measurements. Deterministic tractography with the diffusion tensor model has also been used (Sammartino et al., 2016; Yamada et al., 2010; Barkhoudarian et al., 2010; Sedrak et al., 2011) and is especially useful in easier integration with stereotactic targeting software on the MRI scanner for prospective study (Sammartino et al., 2016).

Tractography-based targeting can be applied in different ways from the implementation in the current study. In one study (Calabrese et al., 2015), high quality postmortem diffusion tractography was used to target Vim and then the detected Vim location was co-registered to the patients' in vivo MR images. Another type of methodologies is to use indirect targeting relative to the location of the tractography reconstructed white matter pathways that run in close proximity but do not intersect the target (Sammartino et al., 2016; Anthofer et al., 2014). Some prior studies have also used tractography to trace from a thalamic target (defined by an atlas or manual delineation, or DBS electrode locations) in an attempt to reconstruct all affected fiber pathways and cortical areas (Barkhoudarian et al., 2010; Sedrak et al., 2011; Klein et al., 2012; Hyam et al., 2012).

In our study, patient P1 exhibits very few streamlines between the thalamus and the hand-knob region in the treated hemisphere. Nonetheless, the tractography results between the thalamus and the hand-knob region in the untreated hemisphere (Fig. 5 first column), and between the thalamus and the motor cortex and the dentate nucleus in both hemispheres are normal, which argues against the possibility of erroneous data acquisition and processing. Interestingly, some of the tremor symptoms of P1 reappeared at 1 year post-treatment, which suggests tractography may have value in predicting which patients will achieve long term benefits from the tcMRgFUS treatment.

An important consideration in our study design was the delineation of the lesion location. For lesion delineation, we aimed to use structural MR images from the imaging time point closest to the treatment date but sufficiently post-treatment such that edema had faded. This corresponded to the 1 year post-treatment.

For our study design we also had to consider the optimal way to use probabilistic tractography results to identify a targeted region. Prior studies have frequently used the voxel with the highest streamline count (Kincses et al., 2012; Pouratian et al., 2011; Jakab et al., 2016; Hyam et al., 2012). Unfortunately, if there are several voxels with streamline counts near the maximum, it is difficult to robustly identify a voxel that represents the focal point of the desired target. Another common approach is to identify a region based on a streamline count threshold (Jakab et al., 2016). One difficulty with this approach is that the choice of threshold is arbitrary and varies significantly across prior studies (e.g. 1% (Klein et al., 2012), 10% (Kincses et al., 2012), or adaptively (Jakab et al., 2016)). Our approach did not rely on identifying the location with the highest streamline count nor an arbitrarily defined threshold. To calculate the overlap between the tractography-identified location and the lesion, we sum the probabilistic streamline count (i.e. the probability of reconstructing streamlines between a thalamic voxel and the hand-knob region) across all voxels within the lesion. This is in contrast to prior studies that thresholded and binarized the probabilistic map and then counted the number of intersected voxels within the lesion (Kincses et al., 2012; Jakab et al., 2016; Klein et al., 2012).

One limitation of the current study is that the clinical outcomes depend not only on the targeting accuracy but also on the success of the tissue ablation. Some measure of maximal temperature achieved during the procedure may help to account for tissue ablation differences but these measurements are currently challenging to achieve with accuracy across multiple MRI slices. Another limitation is the small number of enrolled patients in this clinical trial. Still, retrospective studies such as

this one are a powerful way to evaluate the methodology. Further retrospective studies of tractography-based targeting for tcMRgFUS with larger patient populations could help to determine unified guidelines for the choice of seeds and targets and data quality standards for optimal clinical application.

5. Conclusion

In conclusion, our data supports the use of diffusion tractography to improve the specificity and outcomes of tcMRgFUS targeting for treatment of ET. The diffusion data could be acquired alongside, and used in combination with, the existing pre-treatment imaging that is used to estimate the location of Vim.

Acknowledgements

We thank Drs. Gwenaëlle Douaud and Saad Jbabdi for helpful discussion on diffusion tractography, and Dr. Jingyuan Chen for helpful discussion on statistical analysis. We thank Anne M. Sawyer and Karla Epperson for helping data organization. Funding was provided by the Focused Ultrasound Foundation, InSightec, GE Healthcare, Dana Foundation, National Institutes of Health: P41 EB015891, S10 RR026351, R01 NS095985, R01 MH111444, and German Research Foundation, DFG: TH 2235/1-1.

References

Akram, H., Dayal, V., Mahlknecht, P., Georgiev, D., Hyam, J., Foltynie, T., et al., 2018. Connectivity derived thalamic segmentation in deep brain stimulation for tremor. NeuroImage 18, 130–142.

Anthofer, J., Steib, K., Fellner, C., Lange, M., Brawanski, A., Schlaier, J., 2014. The variability of atlas-based targets in relation to surrounding major fibre tracts in thalamic deep brain stimulation. Acta Neurochir. 156 (8), 1497–1504.

Avants, B.B., Tustison, N.J., Song, G., Cook, P.A., Klein, A., Gee, J.C., 2011. A reproducible evaluation of ANTs similarity metric performance in brain image registration. NeuroImage 54 (3), 2033–2044.

Barkhoudarian, G., Klochkov, T., Sedrak, M., Frew, A., Gorgulho, A., Behnke, E., et al., 2010. A role of diffusion tensor imaging in movement disorder surgery. Acta Neurochir. 152 (12), 2089–2095.

Basser, P.J., Mattiello, J., LeBihan, D., 1994. MR diffusion tensor spectroscopy and imaging. Biophys. J. 66 (1), 259–267.

Behrens, T., Woolrich, M., Jenkinson, M., Johansen-Berg, H., Nunes, R., Clare, S., et al., 2003a. Characterization and propagation of uncertainty in diffusion-weighted MR imaging. Magn. Reson. Med. 50 (5), 1077–1088.

Behrens, T., Johansen-Berg, H., Woolrich, M., Smith, S., Wheeler-Kingshott, C., Boulby, P., et al., 2003b. Non-invasive mapping of connections between human thalamus and cortex using diffusion imaging. Nat. Neurosci. 6 (7), 750–757.

Behrens, T., Berg, H.J., Jbabdi, S., Rushworth, M., Woolrich, M., 2007. Probabilistic diffusion tractography with multiple fibre orientations: what can we gain? NeuroImage 34 (1), 144–155.

Calabrese, E., 2016. Diffusion tractography in deep brain stimulation surgery: a review. Front. Neuroanat. 10, 45.

Calabrese, E., Hickey, P., Hulette, C., Zhang, J., Parente, B., Lad, S.P., et al., 2015. Postmortem diffusion MRI of the human brainstem and thalamus for deep brain stimulator electrode localization. Hum. Brain Mapp. 36 (8), 3167–3178.

Conturo, T.E., Lori, N.F., Cull, T.S., Akbudak, E., Snyder, A.Z., Shimony, J.S., et al., 1999. Tracking neuronal fiber pathways in the living human brain. Proc. Natl. Acad. Sci. 96 (18), 10422–10427.

Dale, A.M., Fischl, B., Sereno, M.I., 1999. Cortical surface-based analysis: I. Segmentation and surface reconstruction. NeuroImage 9 (2), 179–194.

Darian-Smith, C., Darian-Smith, I., Cheema, S.S., 1990. Thalamic projections to sensorimotor cortex in the macaque monkey: use of multiple retrograde fluorescent tracers. J. Comp. Neurol. 299 (1), 17–46.

Descoteaux, M., Deriche, R., Knosche, T.R., Anwander, A., 2009. Deterministic and probabilistic tractography based on complex fibre orientation distributions. IEEE Trans. Med. Imaging 28 (2), 269–286.

Elias, W.J., Zheng, Z.A., Domer, P., Quigg, M., Pouratian, N., 2012. Validation of connectivity-based thalamic segmentation with direct electrophysiologic recordings from human sensory thalamus. NeuroImage 59 (3), 2025–2034.

Elias, W.J., Huss, D., Voss, T., Loomba, J., Khaled, M., Zadicario, E., et al., 2013. A pilot study of focused ultrasound thalamotomy for essential tremor. N. Engl. J. Med. 369 (7), 640–648.

Elias, W.J., Lipsman, N., Ondo, W.G., Ghanouni, P., Kim, Y.G., Lee, W., et al., 2016. A randomized trial of focused ultrasound thalamotomy for essential tremor. N. Engl. J. Med. 375 (8), 730–739.

Fahn, S., Tolosa, E., Marin, C., 1993. Clinical rating scale for tremor. Parkinson's disease and. Mov. Disord. 2, 271–280.

Fang, W., Chen, H., Wang, H., Zhang, H., Puneet, M., Liu, M., et al., 2016. Essential tremor is associated with disruption of functional connectivity in the ventral intermediate nucleus—motor cortex—cerebellum circuit. Hum. Brain Mapp. 37 (1), 165–178.

Federau, C., Goubran, M., Rosenberg, J., Henderson, J., Halpern, C.H., Santini, V., et al., 2017. Transcranial MRI-guided high-intensity focused ultrasound for treatment of essential tremor: a pilot study on the correlation between lesion size, lesion location, thermal dose, and clinical outcome. J. Magn. Reson. Imaging. http://dx.doi.org/10.1002/jmri.25878.

Fischl, B., Sereno, M.I., Dale, A.M., 1999. Cortical surface-based analysis: II: inflation, flattening, and a surface-based coordinate system. NeuroImage 9 (2), 195–207.

Ghanouni, P., Pauly, K.B., Elias, W.J., Henderson, J., Sheehan, J., Monteith, S., et al., 2015. Transcranial MRI-guided focused ultrasound: a review of the technologic and neurologic applications. Am. J. Roentgenol. 205 (1), 150–159.

Henderson, J.M., 2012. "Connectomic surgery": diffusion tensor imaging (DTI) tractography as a targeting modality for surgical modulation of neural networks. Front. Integr. Neurosci. 6, 15.

Hyam, J.A., Owen, S.L., Kringelbach, M.L., Jenkinson, N., Stein, J.F., Green, A.L., et al., 2012. Contrasting connectivity of the ventralis intermedius and ventralis oralis posterior nuclei of the motor thalamus demonstrated by probabilistic tractography. Neurosurgery 70 (1), 162–169.

Jakab, A., Werner, B., Piccirelli, M., Kovacs, K., Martin, E., Thornton, J.S., et al., 2016. Feasibility of diffusion tractography for the reconstruction of intra-thalamic and cerebello-thalamic targets for functional neurosurgery: a multi-vendor pilot study in four subjects. Front. Neuroanat. 10, 76.

Jbabdi, S., Sotiropoulos, S.N., Savio, A.M., Graña, M., Behrens, T.E., 2012. Model-based analysis of multishell diffusion MR data for tractography: how to get over fitting problems. Magn. Reson. Med. 68 (6), 1846–1855.

Jenkinson, M., Beckmann, C.F., Behrens, T.E.J., Woolrich, M.W., Smith, S.M., 2012. FSL. NeuroImage 62 (2), 782–790.

Johansen-Berg, H., Behrens, T.E., Sillery, E., Ciccarelli, O., Thompson, A.J., Smith, S.M., et al., 2005. Functional–anatomical validation and individual variation of diffusion tractography-based segmentation of the human thalamus. Cereb. Cortex 15 (1), 31–39.

Johansen-Berg, H., Gutman, D., Behrens, T., Matthews, P., Rushworth, M., Katz, E., et al., 2008. Anatomical connectivity of the subgenual cingulate region targeted with deep brain stimulation for treatment-resistant depression. Cereb. Cortex 18 (6), 1374–1383.

Jones, E., Wise, S., Coulter, J., 1979. Differential thalamic relationships of sensory-motor and parietal cortical fields in monkeys. J. Comp. Neurol. 183 (4), 833–881.

Kincses, Z.T., Szabó, N., Valálik, I., Kopniczky, Z., Dézsi, L., Klivényi, P., et al., 2012. Target identification for stereotactic thalamotomy using diffusion tractography. PLoS One 7 (1), e29969.

Klein, J., Barbe, M., Seifried, C., Baudrexel, S., Runge, M., Maarouf, M., et al., 2012. The tremor network targeted by successful VIM deep brain stimulation in humans. Neurology 78 (11), 787–795.

Lorenz, D., Schwieger, D., Moises, H., Deuschl, G., 2006. Quality of life and personality in essential tremor patients. Mov. Disord. 21 (8), 1114–1118.

Lorenz, D., Poremba, C., Papengut, F., Schreiber, S., Deuschl, G., 2011. The psychosocial burden of essential tremor in an outpatient- and a community-based cohort. Eur. J. Neurol. 18 (7), 972–979.

Louis, E.D., Ferreira, J.J., 2010. How common is the most common adult movement disorder? Update on the worldwide prevalence of essential tremor. Mov. Disord. 25 (5), 534–541.

Louis, E.D., Ottman, R., 2014. How many people in the USA have essential tremor? Deriving a population estimate based on epidemiological data. Tremor Other Hyperkinet. Mov. 4. http://dx.doi.org/10.7916/D8TT4P4B.

Louis, E.D., Ottman, R., Allen Hauser, W., 1998. How common is the most common adult movement disorder? Estimates of the prevalence of essential tremor throughout the world. Mov. Disord. 13 (1), 5–10.

Matelli, M., Luppino, G., Fogassi, L., Rizzolatti, G., 1989. Thalamic input to inferior area 6 and area 4 in the macaque monkey. J. Comp. Neurol. 280 (3), 468–488.

Modat, M., Ridgway, G.R., Taylor, Z.A., Lehmann, M., Barnes, J., Hawkes, D.J., et al., 2010. Fast free-form deformation using graphics processing units. Comput. Methods Prog. Biomed. 98 (3), 278–284.

Modat, M., Cash, D.M., Daga, P., Winston, G.P., Duncan, J.S., Ourselin, S., 2014. Global image registration using a symmetric block-matching approach. J. Med. Imaging 1 (2), 024003.

Mori, S., Crain, B.J., Chacko, V., Van Zijl, P., 1999. Three-dimensional tracking of axonal projections in the brain by magnetic resonance imaging. Ann. Neurol. 45 (2), 265–269.

Morris, D.M., Embleton, K.V., Parker, G.J., 2008. Probabilistic fibre tracking: differentiation of connections from chance events. NeuroImage 42 (4), 1329–1339.

Nowinski, W., Liu, J., Thirunavuukarasuu, A., 2008. Quantification and visualization of three-dimensional inconsistency of the ventrointermediate nucleus of the thalamus in the Schaltenbrand-Wahren brain atlas. Acta Neurochir. 150 (7), 647–653.

Pierpaoli, C., Basser, P.J., 1996. Toward a quantitative assessment of diffusion anisotropy. Magn. Reson. Med. 36 (6), 893–906.

Pouratian, N., Zheng, Z., Bari, A.A., Behnke, E., Elias, W.J., DeSalles, A.A., 2011. Multi-institutional evaluation of deep brain stimulation targeting using probabilistic connectivity-based thalamic segmentation: clinical article. J. Neurosurg. 115 (5), 995–1004.

Pujol, S., Wells, W., Pierpaoli, C., Brun, C., Gee, J., Cheng, G., et al., 2015. The DTI challenge: toward standardized evaluation of diffusion tensor imaging tractography for neurosurgery. J. Neuroimaging 25 (6), 875–882.

Rouiller, E.M., Liang, F., Babalian, A., Moret, V., Wiesendanger, M., 1994.

Cerebellothalamocortical and pallidothalamocortical projections to the primary and supplementary motor cortical areas: a multiple tracing study in macaque monkeys. J. Comp. Neurol. 345 (2), 185–213.
Rouiller, E.M., Tanne, J., Moret, V., Boussaoud, D., 1999. Origin of thalamic inputs to the primary, premotor, and supplementary motor cortical areas and to area 46 in macaque monkeys: a multiple retrograde tracing study. J. Comp. Neurol. 409 (1), 131–152.
Sakai, S.T., Inase, M., Tanji, J., 2002. The relationship between MI and SMA afferents and cerebellar and pallidal efferents in the macaque monkey. Somatosens. Mot. Res. 19 (2), 139–148.
Sammartino, F., Krishna, V., King, N.K.K., Lozano, A.M., Schwartz, M.L., Huang, Y., et al., 2016. Tractography-based ventral intermediate nucleus targeting: novel methodology and intraoperative validation. Mov. Disord. 31 (8), 1217–1225.
Saranathan, M., Tourdias, T., Bayram, E., Ghanouni, P., Rutt, B.K., 2015. Optimization of white-matter-nulled magnetization prepared rapid gradient echo (MP-RAGE) imaging. Magn. Reson. Med. 73 (5), 1786–1794.
Schell, G.R., Strick, P.L., 1984. The origin of thalamic inputs to the arcuate premotor and supplementary motor areas. J. Neurosci. 4 (2), 539–560.
Schreglmann, S.R., Bauer, R., Hägele-Link, S., Bhatia, K.P., Natchev, P., Wegener, N., et al., 2017. Unilateral cerebellothalamic tract ablation in essential tremor by MRI-guided focused ultrasound. Neurology 88 (14), 1329–1333.
Sedrak, M., Gorgulho, A., Frew, A., Behnke, E., DeSalles, A., Pouratian, N., 2011. Diffusion tensor imaging and colored fractional anisotropy mapping of the ventralis intermedius nucleus of the thalamus. Neurosurgery 69 (5), 1124–1130.
Sotiropoulos, S.N., Jbabdi, S., Xu, J., Andersson, J.L., Moeller, S., Auerbach, E.J., et al., 2013. Advances in diffusion MRI acquisition and processing in the Human Connectome Project. NeuroImage 80, 125–143.
Stejskal, E., Tanner, J., 1965. Spin diffusion measurements: spin echoes in the presence of a time-dependent field gradient. J. Chem. Phys. 42 (1), 288–292.
Stepniewska, I., Sakai, S.T., Qi, H.X., Kaas, J.H., 2003. Somatosensory input to the ventrolateral thalamic region in the macaque monkey: a potential substrate for parkinsonian tremor. J. Comp. Neurol. 455 (3), 378–395.
Tian, Q., Rokem, A., Folkerth, R.D., Nummenmaa, A., Fan, Q., Edlow, B.L., McNab, J.A., 2016. Q-space truncation and sampling in diffusion spectrum imaging. Magn. Reson. Med. 76 (6), 1750–1763.
Torres, C.V., Manzanares, R., Sola, R.G., 2014. Integrating diffusion tensor imaging-based tractography into deep brain stimulation surgery: a review of the literature. Stereotact. Funct. Neurosurg. 92 (5), 282–290.
Tourdias, T., Saranathan, M., Levesque, I.R., Su, J., Rutt, B.K., 2014. Visualization of intra-thalamic nuclei with optimized white-matter-nulled MPRAGE at 7T. NeuroImage 84, 534–545.
Tournier, J.D., Calamante, F., Gadian, D.G., Connelly, A., 2004. Direct estimation of the fiber orientation density function from diffusion-weighted MRI data using spherical deconvolution. NeuroImage 23 (3), 1176–1185.
Traynor, C., Heckemann, R.A., Hammers, A., O'Muircheartaigh, J., Crum, W.R., Barker, G.J., et al., 2010. Reproducibility of thalamic segmentation based on probabilistic tractography. NeuroImage 52 (1), 69–85.
Tuch, D.S., Reese, T.G., Wiegell, M.R., Makris, N., Belliveau, J.W., Wedeen, V.J., 2002. High angular resolution diffusion imaging reveals intravoxel white matter fiber heterogeneity. Magn. Reson. Med. 48 (4), 577–582.
Wedeen, V.J., Hagmann, P., Tseng, W.Y.I., Reese, T.G., Weisskoff, R.M., 2005. Mapping complex tissue architecture with diffusion spectrum magnetic resonance imaging. Magn. Reson. Med. 54 (6), 1377–1386.
Wiesendanger, R., Wiesendanger, M., 1985. Cerebello-cortical linkage in the monkey as revealed by transcellular labeling with the lectin wheat germ agglutinin conjugated to the marker horseradish peroxidase. Exp. Brain Res. 59 (1), 105–117.
Wintermark, M., Druzgal, J., Huss, D., Khaled, M., Monteith, S., Raghavan, P., et al., 2014a. Imaging findings in MR imaging–guided focused ultrasound treatment for patients with essential tremor. Am. J. Neuroradiol. 35 (5), 891–896.
Wintermark, M., Huss, D.S., Shah, B.B., Tustison, N., Druzgal, T.J., Kassell, N., et al., 2014b. Thalamic connectivity in patients with essential tremor treated with MR imaging–guided focused ultrasound: in vivo Fiber tracking by using diffusion-tensor MR imaging. Radiology 272 (1), 202–209.
Woods, S.P., Scott, J.C., Fields, J.A., Poquette, A., Tröster, A.I., 2008. Executive dysfunction and neuropsychiatric symptoms predict lower health status in essential tremor. Cogn. Behav. Neurol. 21 (1), 28–33.
Yamada, K., Akazawa, K., Yuen, S., Goto, M., Matsushima, S., Takahata, A., et al., 2010. MR imaging of ventral thalamic nuclei. Am. J. Neuroradiol. 31 (4), 732–735.
Ye, L., Allen, W.E., Thompson, K.R., Tian, Q., Hsueh, B., Ramakrishnan, C., et al., 2016. Wiring and molecular features of prefrontal ensembles representing distinct experiences. Cell 165 (7), 1776–1788.
Yousry, T., Schmid, U., Alkadhi, H., Schmidt, D., Peraud, A., Buettner, A., et al., 1997. Localization of the motor hand area to a knob on the precentral gyrus. A new landmark. Brain 120 (1), 141–157.
Zesiewicz, T.A., Elble, R., Louis, E.D., Hauser, R.A., Sullivan, K.L., Dewey Jr., R.B., et al., 2005. Practice parameter: therapies for essential tremor: report of the Quality Standards Subcommittee of the American Academy of Neurology. Neurology 64 (12), 2008–2020.